JACS
JOURNAL OF THE AMERICAN CHEMICAL SOCIETY
Article
pubs.acs.org/JACS

Driving Forces for Covalent Assembly of Porphyrins by Selective C−H Bond Activation and Intermolecular Coupling on a Copper Surface

Andrea Floris,[*,†,∥] Sam Haq,[‡] Mendel In't Veld,[‡] David B. Amabilino,[§] Rasmita Raval,[*,‡] and Lev Kantorovich[*,†]

[†]Department of Physics, King's College London, London, Strand WC2R 2LS, United Kingdom
[‡]Surface Science Research Center and Department of Chemistry, University of Liverpool, Liverpool L69 3BX, United Kingdom
[§]School of Chemistry, The University of Nottingham, University Park, Nottingham NG7 2RD, United Kingdom
[∥]School of Mathematics and Physics, University of Lincoln, Brayford Pool, Lincoln LN6 7TS, United Kingdom

Supporting Information

ABSTRACT: Recent synthesis of covalent organic assemblies at surfaces has opened the promise of producing robust nanostructures for functional interfaces. To uncover how this new chemistry works at surfaces and understand the underlying mechanisms that control bond-breaking and bond-making processes at specific positions of the participating molecules, we study here the coupling reaction of tetra-(mesityl)porphyrin molecules, which creates covalently connected networks on the Cu(110) surface by utilizing the 4-methyl groups as unique connection points. Using scanning tunneling microscopy (STM), state-of-the-art density functional theory (DFT), and Nudged Elastic Band (NEB) calculations, we show that the unique directionality of the covalent bonding is found to stem from a chain of highly selective C−H activation and dehydrogenation processes, followed by specific intermolecular C−C coupling reactions that are facilitated by the surface, by steric constraints, and by anisotropic molecular diffusion. These insights provide the first steps toward developing synthetic rules for complex two-dimensional covalent organic chemistry that can be enacted directly at a surface to deliver specific macromolecular structures designed for specific functions.

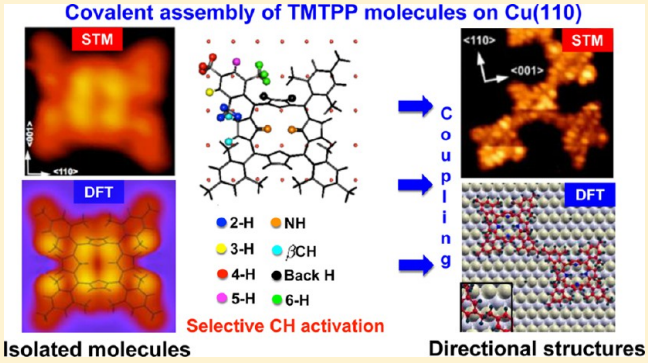

1. INTRODUCTION

Construction of molecular assemblies and networks at surfaces[1,2] provides a highly promising protocol for synthesizing new 2-D materials, delivering new functionalities for biological applications such as sensors and drug delivery[3] and advanced nanotechnology applications in energy harvesting, catalysis, and nanoelectronic devices.[4−6] For many applications, robust networks stabilized by covalent bonds between constituent molecules[1,2,7−12] are technologically more promising, as compared to supramolecular networks stabilized by other types of intermolecular interactions such as H-bonding or van der Waals.[13−19] One broadly applicable approach[2] for the on-surface synthesis of complex and diverse covalent structures is to exploit the prevalence of C−H bonds in organic entities and activate them at a surface to drive intermolecular coupling via C−C or C−metal−C bond formation.[2,12,20,21] However, while this general approach provides broad applicability, there remains a real need to understand and control both the selectivity of C−H bond activation and the intermolecular coupling process so that specific final products are favored, as the first step toward delivering targeted and tailored structures.

Clearly, theory must play a central role in understanding the parameters that govern specific C−H bond activation and the subsequent intermolecular reactions mediated at the surface, hence providing the necessary insights for the experiments. Recently, calculations based on density functional theory (DFT) have started to address the mechanisms underlying the on-surface covalent bonding of molecules in simple cases.[10,22−25] However, for covalent structures involving large and complex organic molecules abundant with C−H bonds, mechanistic details are scarce; here, an important advance would be to predict why, at the given experimental conditions, only particular C−H bonds get activated leading to specific intermolecular connectivities. Such knowledge would underpin future strategies for steering the assembly in the desired direction. To our knowledge, the question of selectivity in the

Received: November 5, 2015
Published: April 20, 2016

DOI: 10.1021/jacs.5b11594
J. Am. Chem. Soc. 2016, 138, 5837−5847

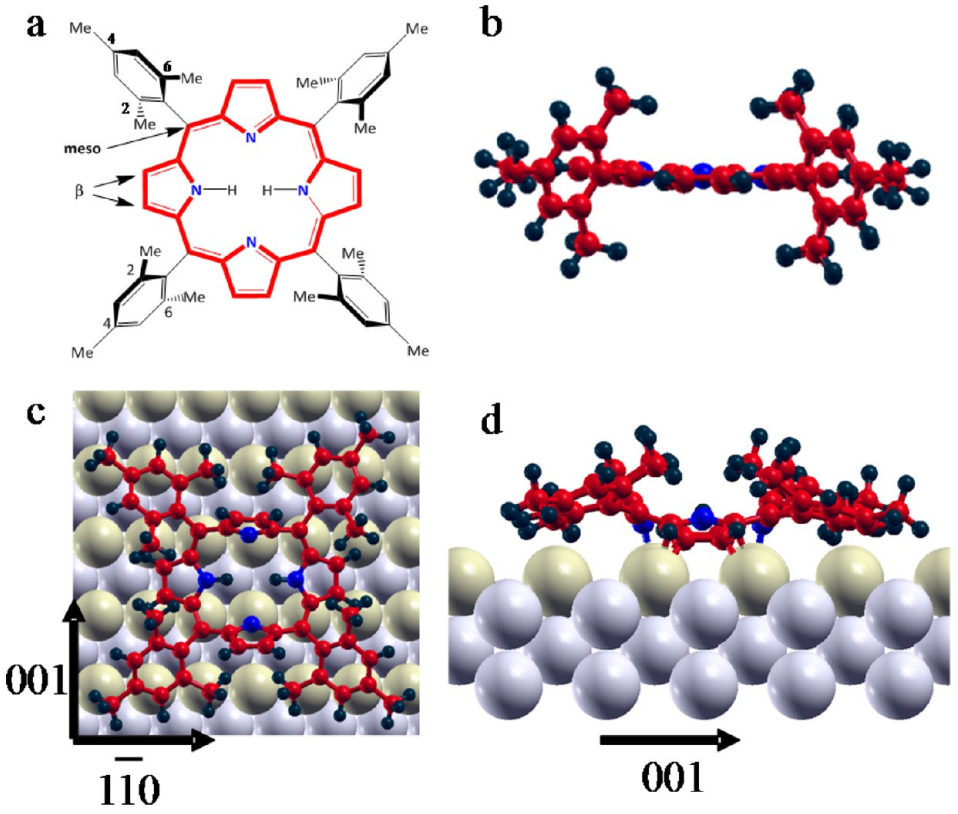

Figure 1. (a) Chemical structure of TMTPP. (b) DFT relaxed configuration in the gas phase (side view) with a flat core and phenyl rings oriented almost perpendicular to it. Top (c) and side (d) views of the energetically most favorable TMTPP adsorption geometry on Cu(110) calculated by DFT showing the alternated orientation of the central pyrrolic groups and the configuration of the phenyl rings. Red, blue, and black spheres correspond to C, N, and H atoms, respectively. Cu atoms in the topmost close-packed rows are shown as light green, while lower lying Cu atoms are gray.

on-surface chemistry mediated only by C−H activation and dehydrogenated (de-H) reactions has not been addressed theoretically before.

In this work, we analyze the general mechanisms underpinning such selectivity by using, as a prototype example, the covalent coupling of tetra-(2,4,6-trimethyl-phenyl)-porphyrin (TMTPP) molecules on the Cu(110) surface, as reported by scanning tunnelling microscopy (STM) experiments.[12] We analyze how upon annealing to 500 K, these rather large molecules, possessing a multitude of external C−H bonds, form uniquely oriented one-dimensional chains and small clusters via specific C−H bond activation. We demonstrate that this high selectivity results from a combination of the intrinsic chemistry of the molecule, the geometry adopted by the molecule at the surface, the catalytic effect of the surface, and specific kinetics associated with underlying processes. All of these effects combine to drive C−H activation, dehydrogenation (de-H), and C−C coupling reactions to occur only at particular methyl groups, explaining the unique molecular connectivity. Finally, we explain the role of annealing in forming the networks and identify the preferential diffusion patterns of TMTPP on this surface, which are paramount in determining the network growth.

2. RESULTS AND DISCUSSION

2.1. Structure of Tetra-(2,4,6-trimethyl-phenyl)-porphyrin (TMTPP) on Cu(110). TMTPP is composed of a porphyrinic tetra-pyrrolic core functionalized at the meso positions by four phenyl rings, each having three methyl groups, two in the carbon atom positions adjacent to the porphyrin (the 2- and 6-positions) and one in the 4-position, as shown in Figure 1a. Our gas-phase DFT calculations show a stable structure with a flat porphyrin core and the planes of the phenyl rings oriented almost perpendicularly to it, Figure 1b.

The molecule is then placed on the Cu(110) surface, consisting of close-packed Cu rows running along the [1$\bar{1}$0] direction, Figure 1c. Periodic DFT calculations show that the presence of the surface strongly modifies the molecular geometry, which undergoes a complex reconfiguration into a structure that is very different from the gas-phase one. The pyrrole rings incorporating the Lewis basic nitrogen atoms lie with their mean plane almost perpendicular to the substrate because of the formation of two N−Cu bonds with the Cu rows, as shown in Figure 1c. In addition, two C−Cu bonds are formed by the −NH-containing pyrrole rings, which are oriented almost horizontally to the surface plane, Figure 1c,d. After a comprehensive DFT analysis of other (∼10) less stable conformations (Figure SI-2), we conclude that the N−Cu and C−Cu covalent links dominate the energetic landscape of the system. In addition, intramolecular interactions are important in determining the final geometry. Each phenyl ring is rotated, with the 6-methyl groups located much closer to the surface than the 2- and the 4-methyl moieties, with the alternating orientations of the pyrrole rings and the planar phenyl group configurations due to the balance between the electrostatic repulsion of the 2- and 6-methyl groups with the core and the steric constraints imposed by the surface, Figure 1c,d. Indeed, our simulations show that in the absence of phenyl groups, the

DOI: 10.1021/jacs.5b11594
J. Am. Chem. Soc. 2016, 138, 5837−5847

core lies completely flat on Cu(110) (Figure SI-3), as reported before.[26] The interplay and optimization of intramolecular interactions and covalent core−surface N−Cu and C−Cu bonds ensure a strong molecule−surface binding, with an adsorption energy of 5.78 eV and a characteristic geometry that is supported by STM data, as discussed below.

Experimental STM images of isolated molecules obtained after adsorption on the Cu(110) surface at 300 K show a rectangular symmetry with two pronounced arc-shaped structures running along the [1$\bar{1}$0] close-packed Cu row direction, Figure 2a. All observed molecules share the same

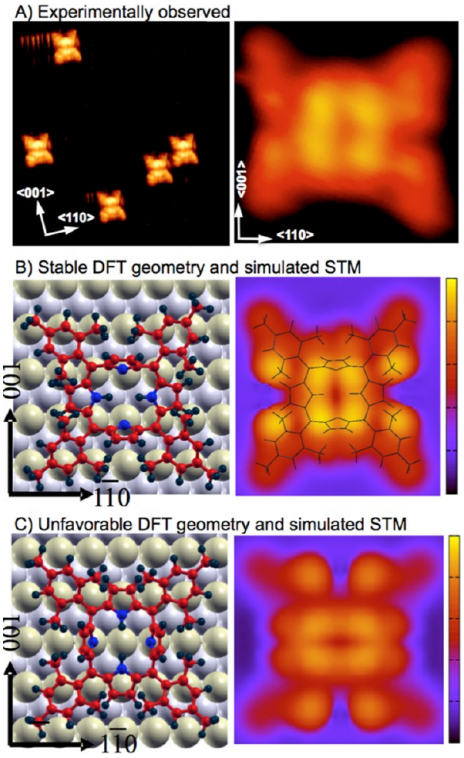

Figure 2. (a) TMTPP molecule on the Cu(110) surface observed in our STM experiments. Left panel: A large-scale image (area 94 × 94 Å^2, V_t = 0.575 V, I_t = 0.34 nA). Right panel: A high-resolution image of a single adsorbed molecule (19 Å^2, −1.03 V, 0.1 nA). (b) The theoretically simulated geometry and the STM image in the most stable geometry. On the right panel, the molecular structure is superimposed on the image to guide the eye. The horizontal arc-shaped protrusions correspond to the vertical pyrroles and the 2-methyl groups, which are the highest molecular chemical groups in the adsorbed molecule. (c) Same as (b), but for an unfavorable geometry, with the STM simulated image in disagreement with the experiment.

submolecular features and a unique orientation relative to the substrate. The images in Figure 2a show the molecules imaged with bright intense lobes around the center of the molecule, arising from the porphyrin core. There is an additional intensity associated with the mesityl groups, which appears in the form of winged lobes (legs). Their orientation with respect to the ⟨110⟩ Cu row direction is found to be exclusively perpendicular, and suggests a unique orientation of the molecule on the surface. To verify the predicted adsorption geometry of Figure 1c,d, STM images were simulated for the most stable and a number of less energetically favorable relaxed geometries.[27,28] The simulated STM images were found to be very sensitive to the TMTPP orientation and structure (Figure 2b,c and Figures SI-4). Importantly, only the geometry corresponding to the most stable structure of Figure 1c,d, with its alternate pyrrole geometries and nonplanar phenyl ring orientation, provides good agreement with the experimental STM images, particularly with respect to the orientation of the winged lobes (legs) relative to the [1$\bar{1}$0] Cu rows, as can be seen by comparing the right panel in Figure 2a with those in Figure 2b,c.

2.2. Surface-Driven Intermolecular Coupling. Experimental STM data show that highly directional macromolecular patterns are formed when TMTPP is adsorbed on Cu(110) and the system annealed to 575 K.[12] Figure 3a shows high-

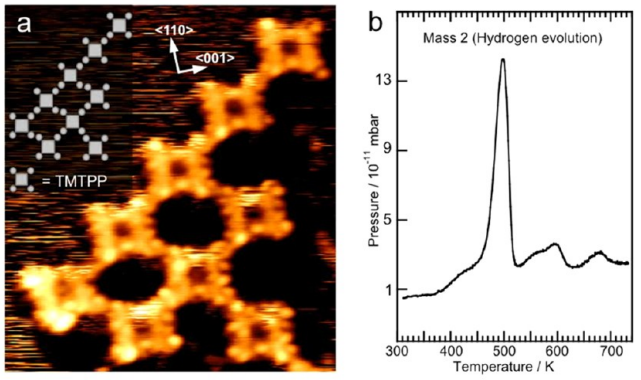

Figure 3. (a) An experimental STM image of a covalently bonded network of TMTPP molecules following heating to 600 K (65 × 73 Å^2, 0.236 V, 0.35 nA). The inset shows a pictorial representation of the networked structure imaged. (b) Temperature-programmed desorption data showing the evolution of H_2 during the coupling process. STM images of larger areas are given in Figure SI-12.

resolution STM data obtained for discrete, covalently linked structures formed by this system. The evolution of H_2 gas was observed between 450 and 520 K (Figure 3b), concomitant with the pattern formation, indicating that dehydrogenation processes accompany the intermolecular bonding associated with the creation of macromolecular structures. TMTPP contains a number of H-containing groups, so three main questions need to be addressed to understand the pattern of reactivity displayed by the system: (i) which H atoms of the molecule are most prone to the dehydrogenation processes; (ii) what are the diffusion patterns of a single molecule on the surface; and (iii) what is the mechanism of the intermolecular bond formation at the surface. Each aspect is considered below.

2.2.1. Selective Dehydrogenation Processes. Using periodic DFT calculations, we identified the dehydrogenation processes that are energetically most favorable, and, thereby, essentially decide the molecular positions that become available for intermolecular covalent bond formation. We start by evaluating the removal energies of each H from the molecule in the gas phase, ΔE_{rem}(gas), Figure 4a. Each ΔE_{rem}(gas) is calculated as the energy difference[29] between the de-H gas-phase molecule and the fully hydrogenated (f-H) gas-phase configuration of Figure 1b. The reaction is endothermic, and a hierarchy of C−H bond breaking energies is obtained as shown in Figure 4a. Specifically, the most favorable hydrogen atoms to remove belong to the 4-, 2-, and 6-methyl groups and to the N−H groups in the central core.[30] These energies reflect the bonding properties of each hydrogen atom within the gas-phase molecule.

DOI: 10.1021/jacs.5b11594
J. Am. Chem. Soc. 2016, 138, 5837−5847

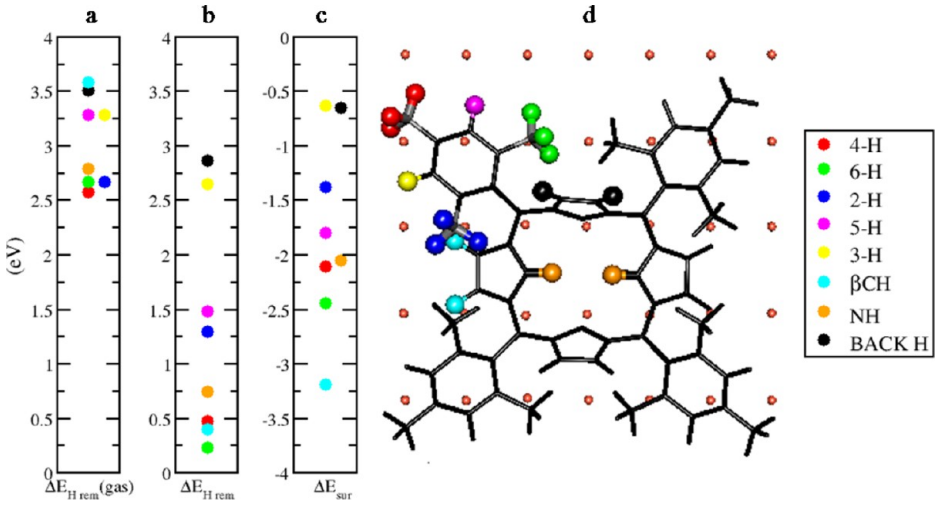

Figure 4. Removal energies of H atoms from nonequivalent positions in TMTPP: (a) in the gas phase, ΔE_{rem}(gas), and (b) adsorbed on Cu(110), ΔE_{rem}; (c) the influence of the surface in each dehydrogenation process is quantified by $\Delta E_{sur} = \Delta E_{rem} - \Delta E_{rem}$(gas). The different types of H atoms are shown in (d) in the molecular structure by the corresponding color code. The removal energies shown are equivalent to dissociation energies; note, the final position of the removed H atoms is on the surface next to the molecule. Although energy barriers for the dehydrogenation reaction provide a better indicator of the ability to dehydrogenate, a systematic calculation of the energy barriers for all nonequivalent H atoms was performed only for the hydrogen atoms from the 4-methyl groups (see Figure 6a). However, it is obvious that the barriers cannot be smaller than the energy difference ΔE_{rem} between the initial and final states; hence, ΔE_{rem} serves as a realistic guide of the ease with which H atoms can be removed from various positions in the molecule. Note that H atoms belonging to a specific methyl group are inequivalent on the surface. However, their removal energies were found to be the same, because the rotational flexibility of the group enables it to relax to the same final configuration.

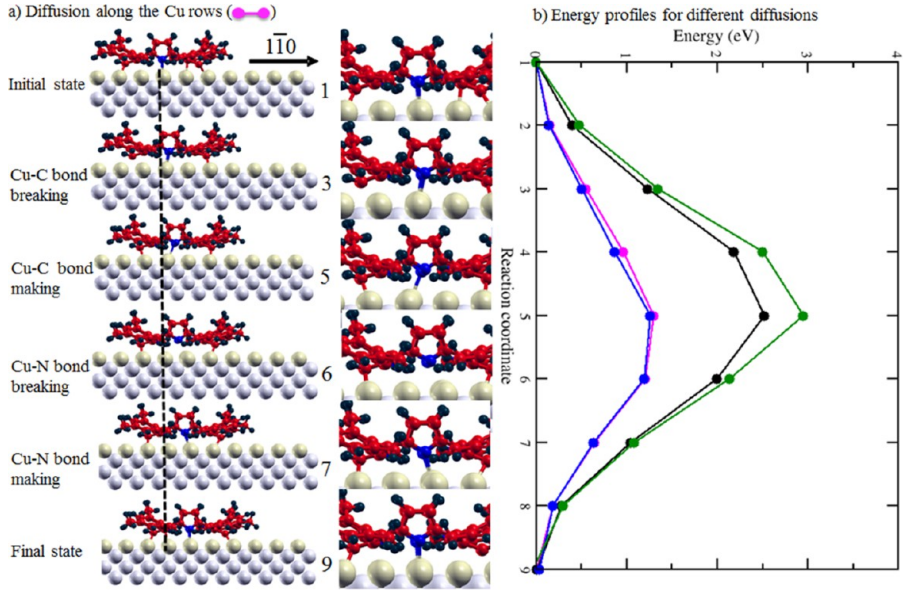

Figure 5. Minimum diffusion paths of a single molecule diffusing on Cu(110) between two stable equivalent configurations (reaction coordinates 1 and 9). (a) A selection of atomic geometries along the path for the fully hydrogenated molecule along the close-packed Cu rows. The black dashed line is a guide for the eye to highlight the diffusion step. Zoom-in of the action areas is shown in the central panel (see also Figure SI-11). (b) Energy profiles along (magenta) and across (black) the Cu rows. The very different energy barriers highlight a strongly anisotropic diffusion, clearly favorable along the rows. Blue and green curves are associated with the diffusion of a dehydrogenated molecule along and across the rows, respectively, showing an increased anisotropy.

To understand the role played by the surface, we calculated the corresponding energy differences ΔE_{rem}, between the fully relaxed de-H and f-H molecular configurations on the surface, for all nonequivalent H atoms, Figure 4b. For the 4-methyl group, we also calculated the dehydrogenation energy barrier (shown in Figure 8, left panel). The removed hydrogen atoms are adsorbed nearby on the surface in the most stable positions bridging two Cu atoms in a row. First, we note that ΔE_{rem} values are significantly lower than the equivalent ΔE_{rem}(gas) values, and that the 4-methyl group energy barrier (~0.70 eV) is also strongly reduced relative to the corresponding H removal barrier in the gas phase (>2.5 eV, Figure 4a), where the barrier and energy difference coincide. These facts demonstrate the catalytic effect of the surface on the dehydrogenations, at least in the most relevant 4-methyl case. Second, the hierarchy of C−H bond breaking is altered significantly from the gas-phase system, and the "easiest" H atoms to remove belong to the 6- and 4-methyl groups and to the horizontal pyrrole C−H

DOI: 10.1021/jacs.5b11594
J. Am. Chem. Soc. 2016, 138, 5837−5847

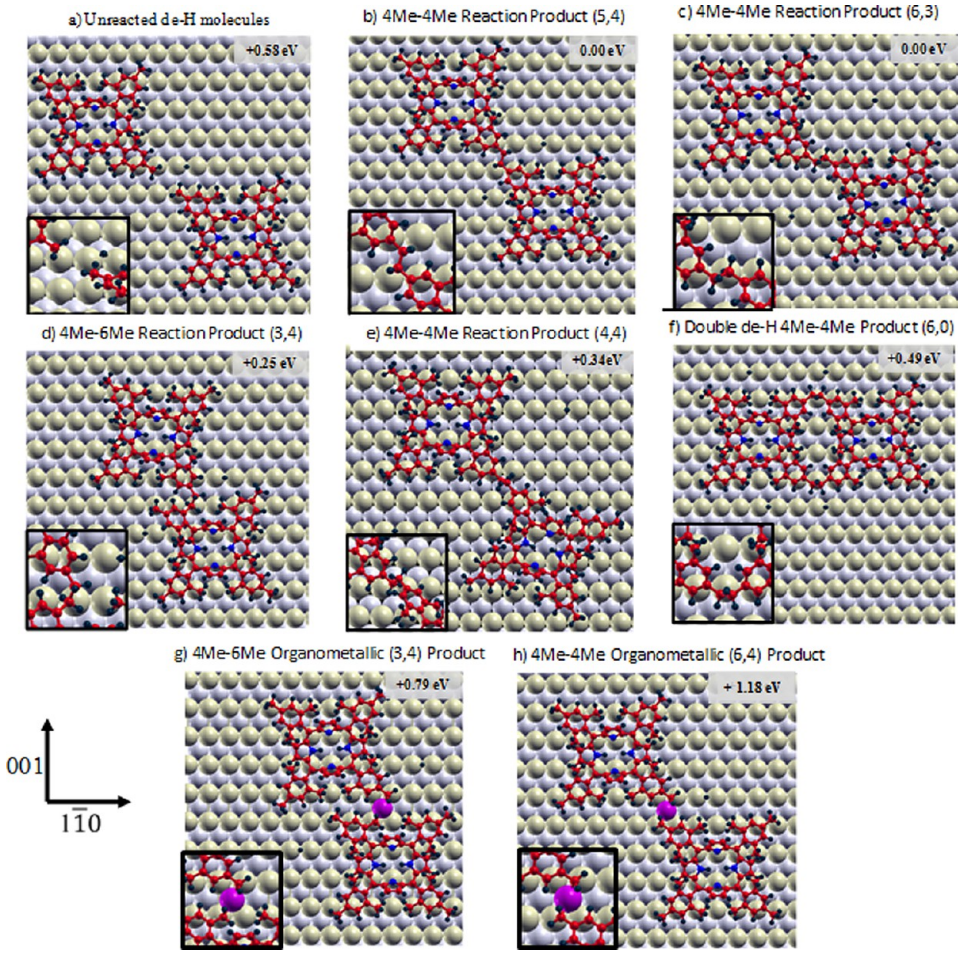

Figure 6. Calculated two molecule structures with their energies given relative to those in structures (b) and (c). (a) Separate and unreacted de-H molecules on the surface. The removed hydrogens are visible some distance away from the molecules in their most stable adsorption geometry on the free surface at $T = 0$ K. (b,c) The most stable geometries of de-H and 4Me-4Me bonded TMTPP molecules on Cu(110), connected via the peripheral 4-methyl groups in their functional phenyl groups. (e) Another configuration having the same intermolecular coupling as in (b) and (c), but with a different arrangement on the surface. (d,f) Differently bonded configurations compatible with steric constraints and an ability of a horizontal diffusion, but energetically less stable than the ones in panels (b) and (c). (g,h) Organometallic-coupled structures, with a Cu adatom (in magenta) mediating the interaction. The insets show the intermolecular bonds in each case.

groups (βCH), all of which lie very close to the Cu surface. This is due to a strong and selective reactivity effect of the surface on these specific dehydrogenation reactions. Thus, the 6- and 4-methyl C−H bonds remain the easiest to break due to both their specific chemistry in the molecule and the activating effect of the surface. Additionally, the horizontal pyrrole C−H groups transform from being the hardest to dissociate in the gas phase to one of the easiest in the adsorbed state due to their proximity to the surface. In contrast, the 2-methyl group becomes relatively harder to break at the surface, as intramolecular interactions orientate the C−H bonds away from the surface plane. We quantify this surface effect in Figure 4c by computing $\Delta E_{sur} = \Delta E_{rem} - \Delta E_{rem}(gas)$, where the lowering of the energy barrier to dehydrogenation is greater for more negative values of ΔE_{sur}.

This leads to the conclusion that in terms of dehydrogenation processes, there are three candidate positions on the molecule, the 6- and 4-methyl and the βCH groups of the horizontal pyrrole, which are important to consider as potential intermolecular linking points for a surface-bound system. Therefore, the following intermolecular connections need to be considered: 4-methyl-4-methyl, 4-methyl-6-methyl, 4-methyl-βCH, βCH-βCH, 6-methyl-6-methyl, and 6-methyl-βCH. Of these, only the first two are sterically allowed, with the experimentally observed final product showing a clear preference for 4-methyl-4-methyl connections where the linked molecules have a diagonal juxtaposition. To understand this clear preference, we need to consider other factors such as molecular diffusion and intermolecular bond formation that are important in guiding the covalent assembly.

2.2.2. Single Molecule Diffusion on Cu(110). The molecule's mobility on the surface is also an essential ingredient for understanding their assembly, as the most probable diffusion patterns may dictate the most likely relative arrangements of connecting molecules and hence bonding topographies. Using the Nudged Elastic Band (NEB) method,[31] we calculated the energy barriers for single molecule diffusion along and across the Cu rows. We find that TMTPP diffuses on the surface by sliding preferentially along the close-packed rows, Figure 5a, where the energy barrier of ~1.3 eV is almost one-half of that across the rows, ~2.5 eV, Figure 5b. This anisotropy in the diffusion pattern reflects the dissymmetry in surface corrugation in the two main directions of the surface.

DOI: 10.1021/jacs.5b11594
J. Am. Chem. Soc. 2016, 138, 5837−5847

Because covalent bonding between molecules may proceed after the dehydrogenation reactions, it is important to understand the mobility of de-H molecules as well. Hence, we simulated the diffusion of a de-H molecule with one H atom removed at the 4-methyl group of the phenyl ring, which corresponds to the experimentally observed connection. Interestingly, we find that the anisotropy of diffusion is enhanced upon dehydrogenation, with the barrier along the rows remaining essentially unchanged, but increasing substantially by ∼0.5 eV across the rows. This effect is attributed to the fact that the de-H molecule forms a C−Cu bond between the dehydrogenated C atom and the nearest Cu atom on the surface, which can easily translate from one Cu atom to the next when diffusion occurs along the close-packed rows, while this is more difficult across the rows due to the larger Cu−Cu distance requiring the C−Cu bond to be completely broken in the transition. We believe that the asymmetry in diffusion we find is general and does not depend on which particular H atom was removed; moreover, we expect that the values of the barriers will not be very sensitive to the position of the removed H atom.

2.2.3. Intermolecular Bonding Configurations. We shall now consider two closely positioned molecules on the surface in a number of geometries that are compatible with the favorable dehydrogenation processes, diffusion along the rows, and sterically allowed covalent products as identified above. Figure 6a shows the relaxed configurations of well separated and unreacted de-H molecules, with the removed H atoms bonded to the free surface in their most stable position some distance away. The relaxed configuration of two separated fully hydrogenated (f-H) molecules was also computed (Figure SI-9). We now consider the 4-methyl-4-methyl (4Me-4Me) coupling product, which arises when the de-H 4-methyl groups at the corresponding molecular corners come into contact, forming a covalent C−C bond. This product can actually be accommodated at the surface in a number of ways. The two most stable and essentially degenerate diagonal arrangements are shown in Figure 6b,c, which differ by a small change in relative positions of the TMTPP components as indicated by the core-to-core surface vectors of (5,4) and (6,3). In both bonded structures, the TMTPP molecules have a configuration and orientation similar to that of the most stable geometry of a single TMTPP molecule on the surface (Figure 1c). Both products are more stable than two unreacted de-H molecules by 0.58 eV, which means that upon dehydrogenation two (or more) approaching molecules are energetically driven to bond. The covalently linked (5,4) and (6,3) accommodated products exhibit a *trans* conformation of the interconnecting 1,2-ethylene group with an intercore distance of ∼19.4 and 19.0 Å, respectively. These connections also lead to slight offsets between the diagonals of the two molecules.[32] Several 4Me-4Me products accommodated in a (4,4) configuration were also calculated (Figure SI-10) with only one energetically driven to bond, with one molecule having a slightly rotated configuration (Figure 6e). However, this geometry is 0.34 eV less energetically favorable than the (5,4) and (6,3) accommodated products.

We also investigated the role of Cu adatoms as possible mediators in organometallic C−Cu−C bonds, as has been observed for other porphyrins at the Cu(110) surface.[2,20,21] A single Cu adatom was placed between the de-H molecules, starting from the relevant configurations in Figure 6b−d. The relaxed structures obtained (Figure 6g,h) were between 0.79 and 1.18 eV higher in energy than those in Figure 6b,c, and hence deemed to be substantially less favorable.[40]

We note that in our DFT calculations, the fully hydrogenated structure of two molecules lies lower in energy than the de-H one by ∼1 eV. Furthermore, the energy of a single H_2 molecule above the surface is less favorable by ∼0.5 eV than that of two well-separated single H atoms adsorbed on it (Figure SI-8). These results imply that both the dehydrogenation process and the recombination of H atoms in the gas phase subsequent to their removal from the surface are not feasible at $T = 0$ K. This is in full agreement with the experiment where the system needs to be heated to over 400 K to initiate the de-H process and observe hydrogen gas evaporation from the surface.

To rationalize these DFT results, one has to compare the free energies of fully hydrogenated and de-H molecules on the surface as a function of temperature (see Supporting Information, section 4). In the de-H case, it is essential to take into account the presence of the H_2 gas above the surface, assumed here to be in thermodynamic equilibrium with the H atoms either adsorbed on the substrate or attached to the molecules. Assuming that the vibrational contribution to the free energy due to H atoms on the surface in all relevant systems is approximately the same, the main contribution to the free energy difference ΔF will come from the difference in DFT energies and from the hydrogen gas free energy. The latter provides an important entropic contribution to ΔF, making the total free energy of dehydrogenation processes favorable at elevated temperatures. Indeed, for the relevant range of T = 500−600 K, we estimate that approximately between −1.8 and −2.2 eV contribution comes from the H_2 gas evaporated into the ultrahigh vacuum chamber at a pressure of 10^{-7} Pa, which is sufficient to reverse the trend of total energies calculated by DFT for the hydrogenated and de-H molecules (see the Supporting Information for details).

The ΔF gain due to H_2 gas is so significant that it can also facilitate dehydrogenation processes from other molecular sites with relatively low removal energies, like the 6-methyl groups and the βCH groups, and hence these events cannot be completely excluded. Assuming diffusion along the Cu rows and a single dehydrogenation per molecule, the only sterically possible bond resulting from these processes is the connection between 4- and 6-methyl groups (4Me-6Me), Figure 6d, accommodated with a core-to-core surface vector of (3,4). It is also worth considering bonded configurations involving two dehydrogenations per molecule and still compatible with diffusion along the rows. One such possibility leads to a horizontal molecular chain, with two adjacent molecules connected by two bonds involving four 4-methyl groups, which has a *cis* conformation of the interconnecting 1,2-ethylene group and a core-to-core surface vector of (6,0), Figure 6f. Additionally, the organometallic products shown in Figure 6g,h might become accessible. However, although ΔF considerations should allow these structures to form, in principle, they are less stable than the 4-methyl-4-methyl products in Figure 6b,c [by 0.25 eV (d), 0.49 eV (f), 0.79 eV (g), and 1.18 eV (h)], and the diffusion barriers to reach them are much higher, as discussed in the next section. We would, therefore, expect these to be minority products.

To establish the types of products created in the experiments, high-resolution STM data were obtained, which allowed both the macromolecular products and the underlying Cu surface atoms to be imaged and core-to-core surface vectors established. Figure 7c,d shows examples of the 4Me-4Me

DOI: 10.1021/jacs.5b11594
J. Am. Chem. Soc. 2016, 138, 5837−5847

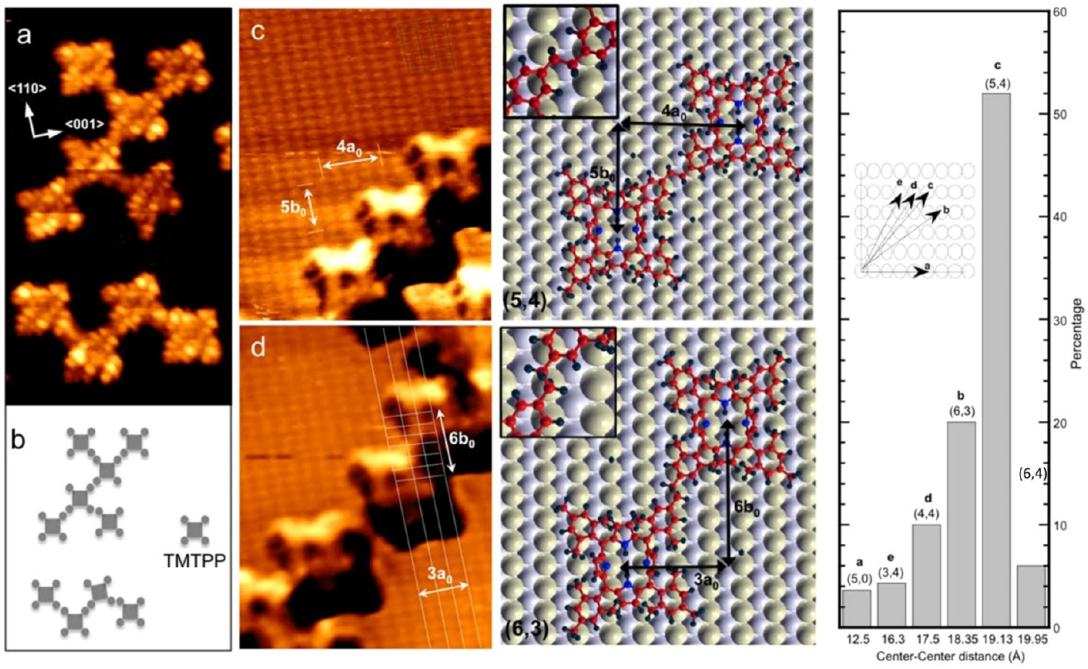

Figure 7. High-resolution STM images showing the connectivity of the reacted TMTPP described in the DFT calculation. (a) The imaged orbital structure is shown (60 × 100 Å^2, 0.284 V, 0.34 nA). (b) A pictorial representation of the networked structure imaged in (a). (c,d) STM images where both the Cu surface atoms and the reacted products are imaged, from which the relative locations of the central cores can be measured (figures on the right of the STM images show the DFT calculated models of these). (c) Three reacted molecules with a (5,4) accommodated configuration are observed (49 × 60 Å^2, 0.311 V, 0.32 nA). (d) Shows molecules arranged in (6,3) accommodated configuration (58 × 68 Å^2 (I_t = 0.37 nA, V = 0.311 V)). The histogram on the right shows center−center molecular distances measured from STM data, compiled from 140 separate connection counts, where both the substrate atoms and the molecular reaction products could be simultaneously imaged. From the data, we calculate an experimental error of ±2% in the measured bond lengths from the exact values expected for each structure.

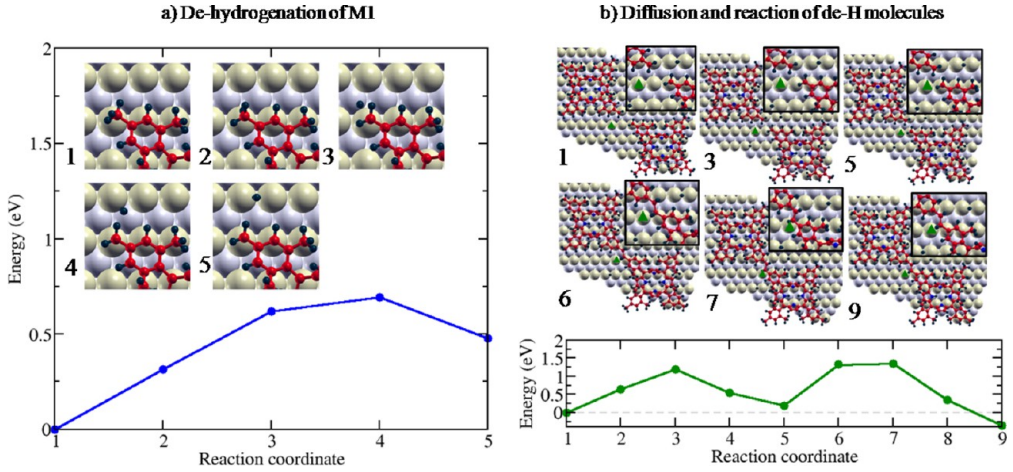

Figure 8. Modeling the "independent" scenario: Minimum energy profile and reaction path bringing two fully hydrogenated molecules, M1 and M2, placed initially far apart on the surface (as in Figure SI-9a), to the bonded configuration as in Figure 6b via the mechanism whereby the two dehydrogenations, diffusion and bonding, happen independently one after another as described in the text. (a) Dehydrogenation reaction involving a 4-methyl hydrogen atom. The initial state (reaction coordinate R_c = 1) is the stable configuration of the intact, fully hydrogenated molecule (reference energy 0 eV). In the final state at R_c = 5, M1 is dehydrogenated, with the removed hydrogen atom placed nearby on the free surface. The reaction path shows how the H atom avoids passing through a higher energy barrier in the central hollow position between 4 topmost Cu atoms. Note that ΔE_{rem} is the difference between the final and initial states. The minimum energy profile for dehydrogenation of M2 is the same. (b) Minimum energy profile and reaction path corresponding to the diffusion of M1 along the Cu rows toward M2 followed by the diagonal bonding between two 4-methyl groups of both molecules. The insets highlight the bonding region. At R_c = 1, the molecules are nonbonded and dehydrogenated. The peak at R_c = 3 stems from the bond breaking with the surface during the M1 diffusion along the row, which at the minimum (R_c = 5) reaches the next equilibrium position. After a further diffusion and initial interaction with M2 (R_c = 6,7), the two molecules eventually connect (R_c = 7−9). The energy gain of the final bonded configuration at R_c = 9 relative to the initial state (R_c = 1) of 0.58 eV indicates that two previously dehydrogenated molecules are driven to connect.

DOI: 10.1021/jacs.5b11594
J. Am. Chem. Soc. 2016, 138, 5837−5847

(5,4) and (6,3) reaction products at the surface. A histogram of the distribution of products with the core-to-core vectors measured from our high-resolution data is shown in Figure 7 (right panel). The data are obtained only when advantageous imaging conditions arise; hence, this represents a small subset of all data collected, and detailed statistical analysis is not possible. Nevertheless, it can be seen that almost 75% of the products possess the 4-methyl-4-methyl (5,4) and (6,3) configurations, which are predicted by theory to be the most favored, and 10% possess the 4-methyl-4-methyl (4,4) configuration (predicted by DFT to be less stable), with good agreement between the measured and calculated intermolecular distances. The minority structures observed correspond to the energetically less favored calculated configurations, with the horizontal chains along the Cu rows observed extremely rarely.

2.3. Simulating the Mechanism of Intermolecular Coupling. We now have all of the ingredients needed for simulating the bonding process itself. We analyze this by means of a sequence of NEB calculations involving two molecules diffusing on the substrate toward each other, with subsequent dehydrogenation at the facing corner sites and then bonding together. In all of our simulations, the molecules are initially fully hydrogenated and placed reasonably far apart in their stable configurations. As the final product geometry, we considered one of the two most favorable de-H bonded pairs shown in Figure 6b, with the two removed H atoms placed well away from the molecules on the free surface.

As described above, single molecule NEB calculations indicate that TMTPP will diffuse mainly along the $[1\bar{1}0]$ rows. Still, several different scenarios are conceivable depending on the order in which dehydrogenation processes happen prior to the bonding. In the simplest case, all elementary processes happen "independently": dehydrogenation of the first molecule (M1), dehydrogenation of the second (M2), their diffusion along the rows, and, finally, bonding. Other more exotic mechanisms, in which the two dehydrogenation events happen at the same time or one slightly after the other, may also be envisaged. For instance, the dehydrogenation of M1 may facilitate the dehydrogenation of M2; that is, the first could catalyze the second. We therefore calculated "synchronous" (two simultaneous) and "asynchronous" (one slightly after the other) dehydrogenation reaction processes (see Supporting Information, section 5 and Figure SI-6 for details). The comparison of the calculated energy barriers predicts that the "independent" scenario described above is by far the most favorable, while the one with synchronous dehydrogenation events is the least. Asynchronous processes lie in between. In Figure 8, we show the main steps for the "independent" scenario, the dehydrogenation reaction for one molecule (a), and the combined diffusion-bonding process of the two de-H molecules (b). This scenario has the effect of splitting the whole process into several elementary steps, each having a low energy barrier. Obviously, when two C−H bonds are broken at the same (or at slightly different) time(s), the corresponding barriers simply add up, which significantly decreases the rate of the whole process as compared to the "independent" mechanism. The same line of reasoning also explains the reduction in diffusion of oligomeric structures as observed by time-resolved STM experiments;[12] this is due to an increased number of N−Cu and C−Cu molecule−surface bonds that have to be broken concomitantly for these larger structures to become mobile on the surface. This also has implications for the growth of the covalent networks in that once a few molecules are bonded together, the ensemble becomes largely stationary, and it is the monomer species that have to diffuse to react with it.

2.4. Overall Reaction Pathway. Overall, the main reaction pathways can be summarized via the following three reactions:

$$(\text{f-H})_s + (\text{f-H})_s \rightarrow (\text{de-H})_s + (\text{de-H})_s + H_s + H_s \quad (1)$$

:

$$H_s + H_s \rightarrow H_{2(s)} \rightarrow H_{2(g)} \quad (2)$$

:

$$(\text{de-H})_s + (\text{de-H})_s \rightarrow (\text{de-H})_{2(s)} \quad (3)$$

:where subscripts (s) and (g) refer to surface-bound and gas-phase species, respectively.

These reactions are depicted in Figure 9, together with the corresponding energetics and energy barriers, for the process corresponding to the formation of the 4Me-4Me (5,4) product species illustrated in Figures 6b and 8b. What we can see from

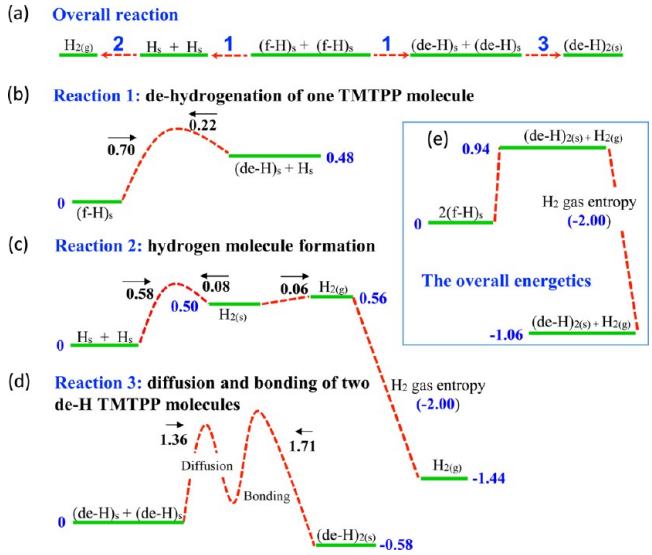

Figure 9. Energetics for the formation of the 4Me-4Me(5,4) product, showing a chain of reactions from two hydrogenated TMTPP molecules, $(\text{f-H})_s$+$(\text{f-H})_s$, to the final bonded structure $(\text{de-H})_{2(s)}$ and a H_2 molecule in the gas phase, $H_{2(g)}$. Relative total energies (in blue) and corresponding energy barriers (in black) with the arrows indicating the direction of each transition are expressed in eV. (a) A schematic showing the general three reactions that represent the overall coupling process. (b) A dehydrogenation reaction of a single TMTPP molecule. (c) A chain of reactions leading to the formation of a hydrogen molecule in the proximity of the surface, $H_{2(s)}$, and then in the gas phase, $H_{2(g)}$, out of two separate H atoms, H_s, adsorbed on the surface (see also Figure SI-14). (d) A reaction leading to the formation of the bonding complex $(\text{de-H})_{2(s)}$ of two dehydrogenated molecules from initially separated dehydrogenated molecules. This reaction requires two activation processes: in the first, the molecules approach each other (diffusion); in the second, they bind (see Figure 8b for details). (e) The overall energy balance: there is an energy penalty of 0.94 eV for dehydrogenating two molecules and bringing a H_2 molecule into the gas phase, which is counterbalanced by the entropy contribution of −2.0 eV, leading to this reaction being energetically favorable by 1.06 eV. The calculated diffusion path of a single H atom on the surface, H_s, is found to have no preferential direction, and the corresponding barrier is ∼0.3 eV (see the Supporting Information for details).

DOI: 10.1021/jacs.5b11594
J. Am. Chem. Soc. 2016, 138, 5837−5847

the energetics of Figure 9 is that the evolution of the hydrogen into the gas phase (see the Supporting Information for details) via reaction 2 is decisive in enabling the overall reaction to become energetically favorable, providing an energy gain of 1.44 eV. However, this process would be common for any of the dehydrogenation sites shown in Figure 4, and therefore it is not discriminating. Hence, the observed selectivity for this system resides in reactions 1 and 3. The energetic cost of reaction 1 depends on the dehydrogenation site on the molecule, and Figure 4b shows that sites 6-H, βCH, 4-H, and NH are the only ones for which the cost of dehydrogenation is sufficiently low so that it can be balanced by the gain due to reaction 2. Turning to reaction 3, βCH and NH can be excluded as connection sites due to steric reasons, and only the 4-H and 6-H sites remain as viable candidates for covalent bonding. 4Me-4Me is the most sterically favorable connection (Figure 6b,c), but the energy gain from reaction 3 is critically determined by how the product is accommodated at the surface, with the (5,4) and (6,3) products being the most stable (Figure 6b,c), while the (4,4) connection is less favorable by 0.34 eV (Figure 6e). A 4Me-6Me bond is sterically possible, but the energy gain of reaction 3 is reduced by 0.25 eV (Figure 6d). The 6Me-6Me connection is sterically disallowed.

The overall energetics and barriers for the 4Me-4Me (5,4) product, Figure 6b, are shown in Figure 9. Here, reaction 1 for the 4-H site is energetically unfavorable (0.96 eV for two molecules; see Figure 4b), while reaction 3 is energetically favorable. However, the gain due to reaction 3 (0.58 eV, Figures 6a,b) does not counterbalance the cost imposed by reaction 1, underlining the role of reaction 2 in making the whole process favorable.

It is also instructive to examine the barriers for the reaction shown in Figure 9. For reaction 1, the dehydrogenation barrier of 0.7 eV for the forward reactions is much greater than the barrier of 0.22 eV for the reverse reaction in which the hydrogen atom, H_s, recombines with the de-H molecule. These barriers seem to suggest that the dehydrogenation process is unlikely. However, the recombination process competes with the diffusion of H_s away from the molecule after dehydrogenation. We find that H_s can diffuse in several directions across the surface with the barrier of ~0.3 eV (see the analysis in the Supporting Information and Figure SI-13), which is similar to the recombination barrier. Thus, the stabilization of the dehydrogenated molecules, $(\text{de-H})_s$, arises from diffusion of the H_s species away from the reaction site. Importantly, we see that the largest barriers are found in reaction 3 for the diffusion and binding of two de-H molecules, and hence this must be the rate-determining step of the overall process. These rather high barriers explain why the formation of the covalent assemblies is only observed at elevated temperatures. Furthermore, the barriers are considerably higher for diffusion of species along the [001] direction as compared to diffusion along the close-packed $[1\bar{1}0]$ rows, and products will largely arise from the latter process.

We now give a detailed characterization of the processes steering the observed covalent assembly of TMTPP molecules on the copper surface. At a high enough temperature, dehydrogenation processes become favorable at specific H sites of the molecules, and these reactions are strongly activated by the substrate. These processes happen independently for different molecules. Fully hydrogenated and dehydrogenated molecules diffuse predominantly along the $[1\bar{1}0]$ close-packed Cu rows with comparable mobilities. When dehydrogenated molecules approach each other along adjoining rows with the phenyl groups capable of making a contact, they are energetically and sterically driven to "connect" through the dehydrogenated $-CH_2$ 4-methyl groups at the corners giving a unique diagonal orientation to the molecular chains, zig-zags and 2-D networks thus formed.[12] The stable bonded configuration in each connected pair has a *trans* 1,2-ethylene unit between the porphyrins, with the coupled molecules retaining a similar orientation as for the unreacted molecule. Other covalent assemblies are significantly disfavored on the basis of energy, steric, and diffusion grounds, and are only rarely observed. For instance, for a covalently linked product to be created parallel along the Cu rows as shown in Figure 6f, four dehydrogenated processes need to happen for two 4-methyl groups of each molecule, which is a low probability event. Even if we assume that the two molecules are already appropriately dehydrogenated, the estimated energy barrier to connect two doubly de-H molecules approaching horizontally along the same rows is found to be more than 1.5 eV higher (Figure SI-7) than for the most favorable diagonal connection, where molecules diffuse along adjoining rows and, furthermore, yield a less stable structure.

3. CONCLUSIONS

In this work, we employed ab initio theory and STM experiments to study the coupling reactions of tetra(mesityl)-porphyrins (TMTPP) adsorbed on the Cu(110) surface. Upon annealing, diagonally oriented covalently bound nanostructures are formed with unique bond directionality. The covalent bonds between molecules are initiated by activation and scission of selected C−H bonds, which leads to the formation of specific and strong C−C intermolecular connections. The main and generic question we have addressed in this work is why only specific C−H bonds are at play in the TMTPP/Cu(110) system leading to highly selective molecular patterns. Using density functional theory, Nudged Elastic Band methods, and appropriate entropic considerations, we provided a detailed explanation of this bond selectivity and of the bonding mechanisms. The selection of the corner 4-methyl groups as activation and binding sites is the result of the interplay of several factors including intrinsic molecular chemistry, adsorption energetics, the selective catalytic effect of the surface, steric effects, and asymmetric diffusion of the molecules on the surface. Entropic effects are also an essential driving force in leading to covalently bound structures at high annealing temperatures.

Growing complex, covalent surface networks in a controlled manner from molecular building blocks represents a real challenge in surface molecular nanoscience. Organic molecules of large size have an abundant number of peripheral C−H bonds, all in principle available for activation, thus providing an attractive "synthon" for coupling strategies. Using selective C−H bond activation is a very promising route in this direction, allowing a diverse range of organic building blocks to be used directly. Our study, albeit on a specific system, provides important insights on the various factors and the underlying driving mechanisms at a surface that affect selective C−H bond scission and specific C−C intermolecular bonding. In particular, we have established that (i) the adsorption and accommodation of the molecule at selected site(s) on the surface are important in dictating the orientation of the C−H functional groups with respect to the surface, which, in turn, influences which specific C−H groups are prone to

DOI: 10.1021/jacs.5b11594
J. Am. Chem. Soc. 2016, 138, 5837−5847

dehydrogenation due to reduction of the reaction barrier, which de-H species are stabilized, and which de-H positions are sterically accessible for intermolecular coupling; (ii) the f-H and de-H molecule−surface interaction and their bond-breaking and bond-making with the surface determine the molecular diffusion barriers and dictate the nature of the species that can participate in the coupling process, with diffusion directions influencing the relative arrangements of connecting molecules; (iii) finally, the accommodation of the coupled product at the surface determines the energetically most favored outcomes. Such knowledge is imperative for establishing a more complete set of future design rules for controlled covalent assembly at surfaces.

4. METHODS

4.1. Computational Details. Density functional theory (DFT) calculations were performed with the Quickstep code[33] within the CP2K package,[34] using a mixed Gaussian and plane waves basis set, the Goedecker, Teter, and Hutter (GTH) pseudopotentials,[35] and a GGA-PBE[36] + rVV10[37] exchange-correlation functional including self-consistently the van der Waals (vdW) interaction. Preliminary calculations made use also of the Grimme D2 functional.[39] We used a plane-wave basis energy cutoff of 400 Ry and the Γ point to sample the Brillouin-zone. The Cu(110) substrate was modeled with a periodically repeated slab of four layers, allowing a vacuum gap between the adsorbed molecule and the bottom layer of the slab above it of ∼7 Å. Relaxations of two molecule system were performed with two layers and were considered completed when atomic forces reached 0.02 eV/Å. Only forces acting on atoms belonging to the two (or one) uppermost top layers and the molecule were used. Nudged Elastic Band (NEB)[31] calculations for single molecule diffusion in Figure 5 were performed using nine replicas, including initial and final states. Figure 8 included five replicas per each individual process. When calculating H removal energies, H atoms were considered for the energy balance as a part of the final systems. Calculated STM images were obtained by calculating the integrated local density of states (ILDOS) within the Tersoff−Hamann method[27] using the plane-wave-pseudopotential package Quantum-ESPRESSO.[38] The constant current STM images were simulated using the LEV00 package.[28]

4.2. Experimental Details. STM experiments were performed under ultrahigh vacuum conditions using a Specs STM 150 Aarhus instrument. The STM was calibrated by measuring the atomic distances of the clean Cu(110) surface. All measurements were taken in constant current mode, using a tungsten tip and at a base pressure of 1.5×10^{-10} mbar. Bias voltages are measured at the sample. The Cu(110) surface was prepared in a UHV chamber using argon ion sputtering and annealing cycles, and atomic flatness and cleanliness were checked by STM prior to dosing the molecule. Tetra-(2,4,6-trimethyl-phenyl)-porphyrin (TMTPP) (Frontier Scientific) was used as purchased and sublimed onto the Cu(110) surface, which was held at room temperature during initial deposition.

■ ASSOCIATED CONTENT

Supporting Information

The Supporting Information is available free of charge on the ACS Publications website at DOI: 10.1021/jacs.5b11594.

Molecular structures on the Cu(110) surface; role of the functional groups in the TMTPP stability on the Cu(110) surface; simulated STM images of a single molecule in several configurations on the surface; free energy comparison of hydrogenated and dehydrogenated structures at finite temperatures; dehydrogenation mechanisms: simultaneous, asynchronous, and independent processes; horizontal bonding of two molecules leading to higher energy barriers; stability of hydrogen on Cu(110) at T = 0 K; unreacted, fully hydrogenated molecules; extra 4-methyl-4-methyl coupled structures; reaction products with higher energy; diffusion along the Cu rows: zoom-in of the bonding area; STM images showing the variety of extended structures; H diffusion on Cu(110); and H_2 molecule formation on Cu(110) and its desorption (PDF)

■ AUTHOR INFORMATION

Corresponding Authors

*an.floris@gmail.com
*r.raval@liverpool.ac.uk
*lev.kantorovitch@kcl.ac.uk

Notes

The authors declare no competing financial interest.

■ ACKNOWLEDGMENTS

Via our membership of the UK's HPC Materials Chemistry Consortium, which is funded by EPSRC (EP/F067496, EP/L000202), this work made use of the facilities of HECTOR and ARCHER, the UK's national high-performance computing service, which is funded by the Office of Science and Technology through EPSRC's High End Computing Programme. A.F. and L.K. thankfully acknowledge the computer resources, technical expertise, and assistance provided by the Red Española de Supercomputación. A.F. thanks Matthew Dyer for discussions. D.B.A. thanks EPSRC for funding. S.H. and R.R. are thankful for the UK EPSRC grant (EP/J019364/1), while A.F. and L.K. are thankful for the EPSRC grant (EP/J019844/1) for funding.

■ REFERENCES

(1) Grill, L.; Dyer, M.; Lafferentz, L.; Persson, M.; Peters, M. V.; Hecht, S. *Nat. Nanotechnol.* **2007**, *2*, 687.
(2) Haq, S.; Hanke, F.; Sharp, J.; Persson, M.; Amabilino, D. B.; Raval, R. *ACS Nano* **2014**, *8*, 8856.
(3) Ludlow, R. F.; Otto, S. *Chem. Soc. Rev.* **2008**, *37*, 101−108.
(4) Smits, E. C. P.; Mathijssen, S. G. J.; van Hal, P. A.; Setayesh, S.; Geuns, T. C. T.; Mutsaers, K. A. H. A.; Cantatore, E.; Wondergem, H. J.; Werzer, O.; Resel, R.; Kemerink, M.; Kirchmeyer, S.; Muzafarov, A. M.; Ponomarenko, S. A.; de Boer, B.; Blom, P. W. M.; de Leeuw, D. M. *Nature* **2008**, *455*, 956−959.
(5) Aida, T.; Meijer, E. W.; Stupp, S. I. *Science* **2012**, *335*, 813−817.
(6) Koepf, M.; Cherioux, F.; Wytko, J. A.; Weiss, J. *Coord. Chem. Rev.* **2012**, *256*, 2872−2892.
(7) Lafferentz, L.; Eberhardt, V.; Dri, C.; Africh, C.; Comelli, G.; Esch, F.; Hecht, S.; Grill, L. *Nat. Chem.* **2012**, *4*, 215.
(8) Cai, J.; Ruffieux, P.; Jaafar, R.; Bieri, M.; Braun, T.; Blankenburg, S.; Muoth, M.; Seitsonen, Ari P.; Saleh, M.; Feng, X.; Müllen, K.; Fasel, R. *Nature* **2010**, *466*, 470−473.
(9) Lee, J.; Dougherty, D. B.; Yates, J. T., Jr. *J. Am. Chem. Soc.* **2006**, *128*, 6008−9.
(10) Treier, M.; Pignedoli, C. A.; Laino, T.; Rieger, R.; Müllen, K.; Passerone, D.; Fasel, R. *Nat. Chem.* **2011**, *3*, 61−67.
(11) Matena, M.; Riehm, T.; Stöhr, M.; Jung, Thomas A.; Gade Lutz, H. *Angew. Chem., Int. Ed.* **2008**, *47*, 2414−2417.
(12) In't Veld, M.; Iavicoli, P.; Haq, S.; Amabilino, D. B.; Raval, R. *Chem. Commun.* **2008**, 1536−1538.
(13) Abdel-Mottaleb, M. M. S.; Gomar-Nadal, E.; Surin, M.; Uji-I, H.; Mamdouh, W.; Veciana, J.; Lemaur, V.; Rovira, C.; Cornil, J.; Lazzaroni, R.; Amabilino, D. B.; De Feyter, S.; De Schryver, F. C. *J. Mater. Chem.* **2005**, *15*, 4601−4615.
(14) Puigmartí-Luis, J.; Minoia, A.; Uji-i, H.; Rovira, C.; Cornil, J.; De Feyter, S.; Lazzaroni, R.; Amabilino, D. B. *J. Am. Chem. Soc.* **2006**, *128*, 12602−12603.

DOI: 10.1021/jacs.5b11594
J. Am. Chem. Soc. 2016, 138, 5837−5847

(15) Abdurakhmanova, N.; Floris, A.; Tseng, T. C.; Comisso, A.; Stepanow, S.; De Vita, A.; Kern, K. *Nat. Commun.* **2012**, *3*, 940.
(16) Floris, A.; Comisso, A.; De Vita, A. *ACS Nano* **2013**, *7* (9), 8059.
(17) Blüm, M.-C.; Ćavar, E.; Pivetta, M.; Patthey, F.; Schneider, W.-D. *Angew. Chem.* **2005**, *117*, 5468−5471.
(18) Tomba, G.; Stengel, M.; Schneider, W.-D.; Baldereschi, A.; De Vita, A. *ACS Nano* **2010**, *4*, 7545−7551.
(19) Della Pia, A.; Riello, M.; Floris, A.; Stassen, D.; Bonifazi, D.; Johnes, Tim S.; De Vita, A.; Costantini, G. *ACS Nano* **2014**, *8* (12), 12356−12364.
(20) Haq, S.; Hanke, F.; Dyer, M. S.; Persson, M.; Iavicoli, P.; Amabilino, D. B.; Raval, R. *J. Am. Chem. Soc.* **2011**, *133*, 12031.
(21) Hanke, F.; Haq, S.; Raval, R.; Persson, M. *ACS Nano* **2011**, *5*, 9093.
(22) Björk, J.; Stafström, S.; Hanke, F. *J. Am. Chem. Soc.* **2011**, *133*, 14884−14887.
(23) Björk, J.; Hanke, F.; Stafström, S. *J. Am. Chem. Soc.* **2013**, *135*, 5768−5775.
(24) Nguyen, M.-T.; Pignedoli, C. A.; Passerone, D. *Phys. Chem. Chem. Phys.* **2011**, *13*, 154−160.
(25) Blankenburg, S.; Rauls, E.; Schmidt, W. G. *J. Phys. Chem. Lett.* **2010**, *1*, 3266−3270.
(26) Dyer, M. S.; Robin, A.; Haq, S.; Raval, R.; Persson, M.; Klimeš, J. *ACS Nano* **2011**, *5*, 1831.
(27) Tersoff, J.; Hamann, D. R. *Phys. Rev. B: Condens. Matter Mater. Phys.* **1985**, *31*, 805.
(28) LEV00 package, http://www.mth.kcl.ac.uk/~lev/codes/lev00/index.html.
(29) Gas-phase energy differences were calculated by both relaxing and not relaxing the molecule after the H removal. However, we present only results obtained without relaxing to avoid "spurious" intramolecular bonds between specific de-H groups and parts of the molecule, which happens during relaxation and significantly alters the reaction coordinate in the gas phase, preventing the energy advantage coming from the surface to be quantified, because it drives a different product outcome.
(30) For a more consistent comparison with the de-H energies of the molecule on Cu(110), where the removed H atom was placed on the bare substrate and its calculated removal energy from the bare surface is 3.3 eV, the ΔE_{rem}(gas) energies were shifted down by 3.3 eV.
(31) Henkelman, G.; Uberuaga, B. P.; Jónsson, H. *J. Chem. Phys.* **2000**, *113*, 9901.
(32) Two different 4-methyl-4-methyl coupling (5,4) and (6,3) structures with a different intermolecular bond orientation were also found having slightly higher energies in comparison with the most stable ones quoted in the text (by +0.1 and +0.35 eV, respectively, Figure SI-9).
(33) VandeVondele, J.; Krack, M.; Mohamed, F.; Parrinello, M.; Chassaing, T.; Hutter, J. *Comput. Phys. Commun.* **2005**, *167*, 103.
(34) http://www.cp2k.org/.
(35) Goedecker, S.; Teter, M.; Hutter, J. *Phys. Rev. B: Condens. Matter Mater. Phys.* **1996**, *54*, 1703.
(36) Perdew, J. P.; Burke, K.; Ernzerhof, M. *Phys. Rev. Lett.* **1996**, *77*, 3865−3868.
(37) Sabatini, R.; Gorni, T.; de Gironcoli, S. *Phys. Rev. B: Condens. Matter Mater. Phys.* **2013**, *87*, 041108.
(38) Giannozzi, P.; Baroni, S.; Bonini, N.; Calandra, M.; Car, R.; Cavazzoni, C.; Ceresoli, D.; Chiarotti, G. L.; Cococcioni, M.; Dabo, I.; Dal Corso, A.; Fabris, S.; Fratesi, G.; de Gironcoli, S.; Gebauer, R.; Gerstmann, U.; Gougoussis, C.; Kokalj, A.; Lazzeri, M.; Martin-Samos, L.; Marzari, N.; Mauri, F.; Mazzarello, R.; Paolini, S.; Pasquarello, A.; Paulatto, L.; Sbraccia, C.; Scandolo, S.; Sclauzero, G.; Seitsonen, A. P.; Smogunov, A.; Umari, P.; Wentzcovitch, R. M. *J. Phys.: Condens. Matter* **2009**, *21*, 395502.
(39) Grimme, S. *J. Comput. Chem.* **2006**, *27*, 1787−1799.
(40) The energy differences involving organometallic structures were computed by comparing their Gibbs free energies (G) with the corresponding ones of the 4Me-4Me (5,4) (Figure 6b) or the 4Me-4Me (6,3) (Figure 6c) configuration. To obtain G, we calculated the adatom chemical potential as $\mu_{Cu} = E_{sur+Cu} - E_{sur}$, where E_{sur+Cu} is the total energy of an isolated Cu atom in its stable position on the surface and E_{sur} is the total energy of the bare surface.

DOI: 10.1021/jacs.5b11594
J. Am. Chem. Soc. 2016, 138, 5837−5847